PUBLICATIONS OF THE ASTRONOMICAL SOCIETY OF THE PACIFIC, **123**:519–530, 2011 May

First Estimates of the Fundamental Parameters of Three Large Magellanic Cloud Clusters

ANDRÉS E. PIATTI

Instituto de Astronomía y Física del Espacio, Casilla de Correo 67, Sucursal 28, 1428, Ciudad de Buenos Aires, Argentina; andres@iafe.uba.ar

AND

JUAN J. CLARIÁ

Observatorio Astronómico, Universidad Nacional de Córdoba, Laprida 854, 5000, Córdoba, Argentina; claria@oac.uncor.edu

MARÍA CELESTE PARISI

Observatorio Astronómico, Universidad Nacional de Córdoba, Laprida 854, 5000, Córdoba, Argentina; celeste@oac.uncor.edu

ANDREA V. AHUMADA

European Southern Observatory, Alonso de Córdova 3107, Santiago, Chile; aahumada@eso.org

Received 2010 December 10; accepted 2011 February 20; published 2011 April 26

ABSTRACT. As part of an ongoing project to investigate the cluster formation and chemical evolution history in the Large Magellanic Cloud (LMC), we have used the CTIO 0.9 m telescope to obtain CCD imaging in the Washington system of NGC 2161, SL 874, and KMHK 1719—three unstudied star clusters located in the outer region of the LMC. We measured T_1 magnitudes and $C - T_1$ colors for a total of 9611 stars distributed throughout cluster areas of 13.6×13.6 arcmin^2. Cluster radii were estimated from star counts distributed throughout the entire observed fields. Careful attention was paid to setting apart the cluster and field star distributions so that statistically cleaned color-magnitude diagrams (CMDs) were obtained. Based on the best fits of isochrones computed by the Padova group to the (T_1, $C - T_1$) CMDs, the δT_1 index, and the standard giant branch procedure, ages and metallicities were derived for the three clusters. The different methods for both age and metallicity determination are in good agreement. The three clusters were found to be of intermediate-age (∼1 Gyr) and relatively metal-poor ($[\mathrm{Fe/H}] \sim -0.7$ dex). By combining the current results with others available in the literature, a total sample of 45 well-known LMC clusters older than 1 Gyr was compiled. By adopting an age interval varying in terms of age according to a logarithmic law, we built the cluster age histogram, which statistically represents the intermediate-age and old stellar populations in the LMC. Two main cluster formation episodes that peaked at $t \sim 2$ and ∼14 Gyr were detected. The present cluster age distribution was compared with star formation rates that were analytically derived in previous studies.

Online material: extended tables

1. INTRODUCTION

The Large Magellanic Cloud (LMC) has long been a favorite laboratory, providing us not only with valuable information about its own complex star formation history (SFH), but also with important clues for understanding the formation and evolution of distant galaxies. Although the estimated number of LMC star clusters is ∼4200 (Hodge 1988), this number may be significantly larger if emission-free associations and objects related to emission nebulae are included (Bica et al. 1999). However, the number of well-studied LMC clusters is still a very small fraction of those that have so far been catalogued.

In the present study, we employ the Washington photometric system. Initially developed for late-type stars and ancient stellar populations (Canterna 1976), this system has been widely applied to star clusters covering a wide age range in our Galaxy and in the Magellanic Clouds (see, e.g., Parisi et al. 2005; Piatti et al. 2007a). The long-wavelength baseline covered by the Washington filters can provide a good insight into color-magnitude diagrams (CMDs) of young, intermediate-age, and old star clusters, especially since the development of Washington system isochrones (Lejeune & Schaerer 2001; Girardi et al. 2002) allows us to determine cluster ages. Another valuable result that the Washington system allows us is to estimate clusters' ages and giants' metallicities. The ages and metallicities of LMC star clusters are reliable indicators of the chemical evolution and SFH in the LMC. In particular, the measurement of

these two parameters for a large number of clusters is required to trace the details of the recent bursts in cluster and star formation that occurred over the last few billion years. Unfortunately, the well-known pronounced cluster age gap from ~3 to 9 Gyr (see, e.g., Geisler et al. 1997) constitutes an obstacle in the use of the clusters to probe the chemical enrichment and SFH of the LMC in detail during this long period of apparent quiescence.

In the last decade, much effort has been devoted to the study of young, intermediate-age, and old LMC star clusters using the Washington system (e.g., Geisler et al. 2003; Piatti et al. 2003a, 2007a, 2009). The present study deals with Washington photometry of three LMC star clusters located in the outer disk region, namely, NGC 2161, SL 874, and KHMK 1719. Bica et al. (1996) obtained integrated UBV photometry for NGC 2161 and SL 874 and derived equivalent SWB VI types (Searle et al. 1980) for these two clusters from their location in the $(U-B)$ vs $(B-V)$ diagram. The SWB sequence is primarily related to age (e.g., Elson & Fall 1985; Chiosi et al. 1988). In particular, the SWB type VI clusters are known to be comparable with Galactic clusters with ages in the 2–5 Gyr range. We are aware of no other CMDs for any of these clusters nor of any other age or metallicity determinations. The current study is part of a series of systematic studies of LMC star clusters carried out as uniformly as possible using the same telescope, detector, and photometric system. We aim at deriving ages and metallicities for the aforementioned star clusters and at combining these newly obtained results with those of our previous studies of the LMC, made using the same technique. In some cases, we have even been able to study the field stellar populations surrounding LMC clusters.

This article is organized as follows. Section 2 describes observations and data reduction. Section 3 focuses on describing the main features of the CMDs and the method applied to minimize field star contamination. In this section, we also describe how cluster sizes are determined from their stellar density profiles. Reddenings, ages, and metallicities for the three selected clusters are derived in § 4, while the analysis and discussion of the results are presented in § 5, together with a thorough discussion of the age distribution of LMC star clusters older than 1 Gyr. Our main findings are summarized in § 6.

2. DATA COLLECTION AND REDUCTION

We obtained images for the three selected clusters on the nights of 2004 December 17 and 18 with a 2048×2048 pixel Tektronix CCD attached to the 0.9 m telescope (scale $0.396''$ pixel^{-1}) at Cerro Tololo Inter-American Observatory (CTIO), Chile. Its field of view is 13.6×13.6 arcmin^2. We controlled the CCD through the CTIO ARCON 3.3 data acquisition system in the standard quad amplifier mode. We used the Washington C (Canterna 1976) and Kron-Cousins R filters to be consistent with our previous studies. The R filter has a significantly higher throughput as compared with the standard Washington T_1 filter so that R magnitudes can be accurately transformed to yield T_1 magnitudes (Geisler 1996). In particular, this filter combination allowed us to derive accurate metallicities based on the standard giant branch technique outlined in Geisler & Sarajedini (1999). We obtained a series of bias, dome, and sky flat-field exposures per filter to calibrate the CCD instrumental signature. We also obtained images for the Small Magellanic Cloud (SMC) clusters L 110 and L 112, which were previously observed at La Silla (ESO, Chile) with the C and T_1 filters (Piatti et al. 2007b). L 110 and L 112 were used only as control clusters to verify the quality of the CTIO photometry. Table 1 shows the log of the observations with filters, exposure times, air masses, and seeing estimates. A large number (typically 20) of standard stars from the list of Geisler (1996) was also observed on each night. Care was taken to cover a wide color and air-mass range for these standards in order to bracket and properly calibrate the program stars observed on these nights.

We applied bias subtraction to all the images and flat fielding to both standard and program field images, employing weighted combined signal-calibrator frames and standard observational techniques and tasks in IRAF.[1] The resulting processed images turned out to be satisfactorily flat. We then derived the instrumental magnitudes for the standard stars from aperture photometry using DAOPHOT/IRAF routines (Stetson et al. 1990). We obtained the following mean transformation equations between instrumental and standard magnitudes through least-squares fits:

$$c = (3.679 \pm 0.021) + T_1 + (C - T_1) + (0.294 \pm 0.014) \times X_C - (0.085 \pm 0.005) \times (C - T_1), \quad (1)$$

$$r = (3.206 \pm 0.021) + T_1 + (0.115 \pm 0.014) \times X_{T_1} - (0.014 \pm 0.004) \times (C - T_1), \quad (2)$$

where X represents the effective air mass. Capital and lowercase letters stand for standard and instrumental magnitudes, respectively. The coefficients were derived through the IRAF routine `FITPARAM`. The resulting rms errors are 0.021 for c and 0.014 for r, which indicates that the nights were photometric.

The stellar photometry was performed using the star-finding and point-spread-function (PSF) fitting routines in the DAOPHOT/ALLSTAR suite of programs (Stetson et al. 1990). For each frame, a quadratically varying PSF was derived by fitting ~100 stars, once the neighbors were eliminated by using a preliminary PSF. Such preliminary PSF was obtained from the brightest, least contaminated 35–40 stars. Both groups of PSF stars were interactively selected. We then used the ALLSTAR

[1] IRAF is distributed by the National Optical Astronomy Observatories, which is operated by the Association of Universities for Research in Astronomy, Inc., under contract with the National Science Foundation.

TABLE 1
OBSERVATION LOG OF SELECTED CLUSTERS

Star cluster [a]	α_{2000} (h m s)	δ_{2000} (° ′ ″)	l (°)	b (°)	Date	Filter	Exposure (s)	Air mass	Seeing (″)
L 110, ESO 29-SC48	1 34 26	−72 52 28	298.56	−43.89	Dec. 18	C	2400	1.40	1.5
						R	900	1.46	
L 112	1 35 58	−75 27 28	299.23	−41.35	Dec. 17	C	2400	1.46	1.8
						R	900	1.50	1.7
NGC 2161, SL 789, LW 337,						C	2400	1.40	1.8
ESO 33-SC31, KMHK 1544	5 55 42	−74 21 14	285.38	−29.79	Dec. 18	R	900	1.42	1.6
SL 874, LW 446,ESO 57-SC77,	6 15 57	−70 04 23	280.43	−28.39	Dec. 17	C	2400	1.30	1.6
KMHK 1713						R	900	1.34	1.4
KMHK 1719	6 17 19	−70 03 39	280.42	−28.27	Dec. 17	C	2400	1.30	1.6
						R	900	1.34	1.4

[a] Cluster identifications from (L): Lindsay 1958; (ESO): Lauberts 1982; (SL): Shapley & Lindsay 1963; (LW): Lyngå & Westerlund 1963; (KMHK): Kontizas et al. 1990.

program to apply the resulting PSF to the identified stellar objects and to create a subtracted image that was used to find and measure magnitudes of additional fainter stars. This procedure was repeated three times for each frame. Finally, we computed aperture corrections from the comparison of PSF and aperture magnitudes using the neighbor-subtracted PSF star sample. The resulting aperture corrections were, on average, less than 0.02 mag (absolute value) for c and r images, respectively.

We combined all the independent measurements using the standalone DAOMATCH and DAOMASTER programs. The final information gathered for each cluster consists of a running number per star, the x and y coordinates, the measured T_1 magnitudes, $C - T_1$ colors, and the observational errors $\sigma(T_1)$ and $\sigma(C - T_1)$. Tables 2 to 6 give this information for the SMC control clusters L 110 and L 112 and for the LMC clusters NGC 2161, SL 874, and KMHK 1719, respectively. Tables 2–6 are published in their entirety in the electronic edition of the *PASP*. A portion is shown here for guidance regarding their form and content.

We first examined the quality of our photometry in order to evaluate the influence of the photometric errors on the cluster fiducial characteristics in the CMDs. The behavior of the T_1 magnitude and $C - T_1$ color errors as a function of T_1 for the SL 874 field—the most populous field in the sample—is shown in Figure 1. Such behavior is typical in our photometry. Thus, we were allowed to detect and measure the turn-off (TO) for all the program clusters, which was used in our age estimates. Indeed, by using the relation between the TO R magnitude and age according to theoretical isochrones by Girardi et al. (2002) and by comparing it with our data, we concluded that we are able to define TOs for stellar populations as old as 3 ± 1 Gyr ($R \approx 21.0$) with an error of ∼0.10 in R. Slightly fainter TOs can be reached at the expense of larger errors. Figure 2 presents the results of the comparison between the photometry of L 110 and L 112 by Piatti et al. (2007b) and the present one, measured by the differences $\Delta T_1 = T_{1_{\rm pub}} - T_{1_{\rm this\ work}}$ and $\Delta(C - T_1) = (C - T_1)_{\rm pub} - (C - T_1)_{\rm this\ work}$, which were computed for a total of 1288 common stars. The resulting ΔT_1 and $\Delta(C - T_1)$ values turned out to be -0.022 ± 0.068 and 0.002 ± 0.022, respectively.

3. ANALYSIS OF THE COLOR-MAGNITUDE DIAGRAMS

In Figure 3 we show the CMD of all the measured stars—error bars included along the right margin—in the field of SL 874, which is the most populated observed field (6136 stars). The two remaining cluster fields exhibit CMDs with fairly similar characteristics. A mixture of young and old stellar populations clearly appear to be the main LMC field features of the CMDs. The most obvious traits are the populated old main sequence (MS), the populous and broad subgiant branch—an indicator of the evolution of stars with ages (masses) within a nonnegligible range—the red clump (RC), and the red giant

TABLE 2
CCD CT_1 DATA OF STARS IN THE FIELD OF L 110

ID	x (pixels)	y (pixels)	T_1 (mag)	$\sigma(T_1)$ (mag)	$C - T_1$ (mag)	$\sigma(C - T_1)$ (mag)
899	231.913	864.505	18.012	0.008	1.163	0.015
900	1078.635	865.152	18.631	0.011	1.598	0.030
901	1309.083	866.052	20.827	0.060	0.362	0.095

TABLE 3
CCD CT_1 DATA OF STARS IN THE FIELD OF L 112

ID	x (pixels)	y (pixels)	T_1 (mag)	$\sigma(T_1)$ (mag)	$C-T_1$ (mag)	$\sigma(C-T_1)$ (mag)
120	1965.339	453.250	18.814	0.039	1.494	0.055
121	1273.965	2039.336	18.548	0.013	1.343	0.029
122	1483.983	472.096	16.942	0.004	2.130	0.016

branch (RGB). The RC is somewhat elongated in T_1 and appears to be populated at brighter magnitudes by the so-called vertical red clump structure (Zaritsky & Lin 1997; Gallart 1998; Ibata et al. 1998). In addition, there is some evidence of the vertical structure stars seen by Piatti et al. (1999) in some LMC fields.

Since all the CMDs reveal both cluster and field star characteristics that are more or less superimposed, we should first separate the cluster stars from those belonging to the surrounding fields in order to estimate the cluster fundamental parameters from their CMDs. Note that both cluster and field stars are affected by nearly the same interstellar reddening, which is indeed what causes the overlapping of their MSs. This fact makes the cleaning of the CMDs even more difficult.

To filter the field stars from the CMDs, we applied a statistical procedure. Such method consists of first adopting three CMDs from different regions located far from the clusters. The dimensions of each selected field region were 600×600 pixels and acted as reference to statistically filter an equal area centered on the clusters. In general, the clusters expand over areas smaller than ~200 pixels in radius.

Second, using each field CMD independently, we counted how many stars lie in different magnitude-color bins with sizes $[\Delta T_1, \Delta(C-T_1)] = (0.25, 0.1)$, (0.25,0.2), (0.5,0.1), and (0.5,0.2) mag, respectively. Then we subtracted the number of stars counted for each bin of the field $[T_1, (C-T_1)]$ CMDs from their cluster regions. Thus, we removed those stars closer in magnitude and color to the ones in the star fields. We obtained, therefore, 12 different subtracted CMDs for each cluster field. With the aim of comparing the resulting residuals, we applied this filtering procedure by also using the four bin sets shifted by half of their sizes. This method rendered 24 additional tables for each observed cluster field that are similar to Tables 2 to 6. Each of them contains the stars that have not been subtracted within the cluster region, since we eliminated those matching the spatial density, magnitude, and color distributions of the selected star fields.

Finally, we adopted the cluster CMDs of those generated with stars appearing in the corresponding 24 tables. In order to illustrate the statistical cleaning procedure, Figures 4 to 6 show (*left top*) close-up schematic finding charts of NGC 2161, SL 874, and KMHK 1719, respectively. They were drawn using all the measured stars in the different fields. The sizes of the plotting symbols are proportional to the T_1 brightness of the stars. In the right top panels, we display the CMDs for stars distributed within the top left panels, while the cleaned cluster CMDs are presented in the right bottom panels. Equal close-up cluster area field CMDs are shown in the left bottom panels. In all the CMDs we included error bars along the right margins.

When comparing field and cleaned cluster CMDs, differences in stellar composition become noticeable, as can be seen in both bottom panels of Figures 4 to 6. Particularly, the RC field at $T_1 \sim 18.5$–19 (which becomes prominent for age ~1–5 Gyr), is the most common field feature, besides the field MS composed of stars within a relatively old age range. The CMDs of NGC 2161, SL 874, and KMHK 1719 ,which exhibit a clear development of the red giant star phases, resemble those of intermediate-age star clusters.

In order to build density profiles of the observed clusters, we began by fitting Gaussian distributions to the star counts in the x and y directions to determine the coordinates of the cluster centers and their estimated uncertainties. The number of stars projected along the x and y directions were counted using 5 pixel intervals, which allowed us to statistically sample the spatial distributions. The fit of a single Gaussian for each projected density profile was performed using the `NGAUSSFIT` routine in the STSDAS/IRAF package. The cluster centers were determined with a typical `NGAUSSFIT` standard deviation of ± 5 pixels (~2″). We then constructed the cluster radial profiles by computing the number of stars per unit area at a given radius r,

TABLE 4
CCD CT_1 DATA OF STARS IN THE FIELD OF NGC 2161

ID	x (pixels)	y (pixels)	T_1 (mag)	$\sigma(T_1)$ (mag)	$C-T_1$ (mag)	$\sigma(C-T_1)$ (mag)
106	776.881	67.425	19.002	0.012	1.467	0.027
107	782.966	67.512	18.021	0.009	1.988	0.017
108	1180.381	68.880	17.580	0.005	2.415	0.016

TABLE 5
CCD CT_1 DATA OF STARS IN FIELD OF SL 874

ID	x (pixels)	y (pixels)	T_1 (mag)	$\sigma(T_1)$ (mag)	$C-T_1$ (mag)	$\sigma(C-T_1)$ (mag)
88	911.112	92.024	18.416	0.009	1.550	0.021
89	1411.709	92.658	16.380	0.004	2.954	0.013
90	1624.128	92.701	19.449	0.020	1.586	0.046

as shown in Figure 7. The radius corresponding to the FWHM ($r_{\rm FWHM}$) and the cluster radius ($r_{\rm cls}$)—defined as the distance from the cluster's center where the number of stars equals that of the background—are listed in Table 7. Assuming that the LMC is located at a distance of around 50 kpc (Subramanian & Subramanian 2010), we computed the linear values in parsecs for $r_{\rm FWHM}$ and $r_{\rm cls}$, respectively. As the tidal radius is much larger than the core radius in each cluster, the latter may be taken as the radius at which the stellar density profile has dropped to half its central value. For LMC clusters, the ratios of tidal to core radii range between 10 and 100 (Elson et al. 1987). Thus, adding the $r_{\rm FWHM}$ values of Table 7 to the results shown in Figure 14 of Mackey & Gilmore (2003), we estimated that NGC 2161, SL 874, and KMHK 1719 might not be younger than ∼500, 50, and 20 Myr, respectively.

4. ESTIMATES OF THE CLUSTERS' FUNDAMENTAL PARAMETERS

Cluster reddening values were estimated by interpolating the extinction maps of Burstein & Heiles (1982, hereafter BH). BH maps were obtained from H I (21 cm) emission data for the southern sky and provide us with foreground $E(B-V)$ color excesses, which depend on the Galactic coordinates. More recently, Schlegel et al. (1998, hereafter SFD) obtained full-sky maps from 100 μm dust emission. They found that the dust map correlates well with maps of H I emission at high latitudes, but deviations are coherent in the sky and are especially conspicuous in regions of saturation of H I emission toward denser clouds (Piatti et al. 2003a, 2008). The color excesses in certain regions of the sky are not uniform at all, and so we used the SFD's reddening maps to corroborate its uniformity across the observed fields. We computed $E(B-V)_{\rm SFD}$ color excesses for grids in the (l,b) Galactic coordinate plane, with steps of $\Delta(l,b)=(0.01°,0.01°)$, thus covering the whole observed fields. We obtained between 80 and 100 color excess values per cluster field. Then, for the resulting $E(B-V)_{\rm SFD}$ values, we built histograms and calculated their centers and FWHM values. Since the FWHM values turned out to be considerably small, we assumed that the interstellar absorption is uniform across the cluster fields. Table 8 lists the $E(B-V)_{\rm BH}$ color excesses, the minimum and maximum $E(B-V)_{\rm SFD}$ values, and the adopted cluster reddening values. The $A_{T_1}/E(B-V)$ and $E(C-T_1)/E(B-V)$ ratios given by Geisler & Sarajedini (1999) were then used to enter the CMDs with the corresponding M_{T_1} and $(C-T_1)_o$ values.

As for the cluster distance moduli for all the clusters, we adopted the value of the LMC distance modulus $(m-M)_o = 18.50 \pm 0.10$ recently reported by Saha et al. (2010). On the other hand, Subramanian & Subramanian (2009) found that the average depth for the LMC disk is 3.44 ± 1.16 kpc. Bearing in mind that any cluster of the present sample could be placed in front of, or behind, the main body of the LMC, we conclude that the difference in apparent distance modulus could be as large as $\Delta(V-M_V) \sim 0.3$ mag, if a value of 50 kpc is adopted for the mean LMC distance. Given the fact that we estimate an uncertainty of 0.2–0.3 mag when adjusting the isochrones to the cluster CMDs in magnitude, our simple assumption of adopting a unique value for the distance modulus of all the clusters should not dominate the error budget in our final results. In fact, when overplotting the zero-age main sequence (ZAMS) on the observed cluster CMDs, previously shifted by the $E(B-V)$ of Table 8 and by $(m-M)_o = 18.50$, we generally found an excellent match. In order to estimate the ages of the three clusters, it must be taken into account that cluster metallicity plays an important role when fitting theoretical isochrones. Indeed, theoretical isochrones of the same age but with different metallicities may be either slightly or remarkably different. The distinction is mainly evident for the evolved RC and RGB phases. The ZAMS shown in each case is less affected by

TABLE 6
CCD CT_1 DATA OF STARS IN FIELD OF KMHK 1719

ID	x (pixels)	y (pixels)	T_1 (mag)	$\sigma(T_1)$ (mag)	$C-T_1$ (mag)	$\sigma(C-T_1)$ (mag)
192	945.794	124.353	18.621	0.009	1.878	0.022
193	443.227	124.357	18.604	0.015	1.529	0.025
194	1904.460	124.381	18.932	0.031	1.367	0.041

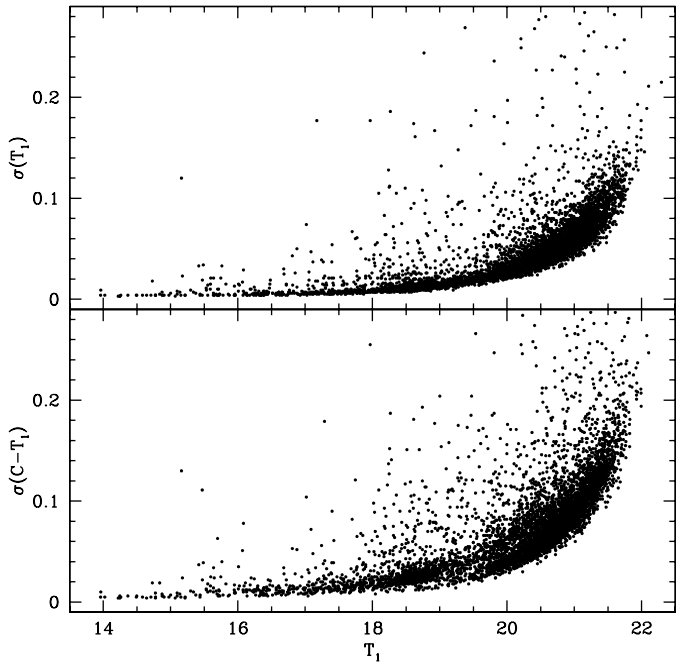

FIG. 1.—Magnitude and color photometric errors as a function of T_1 for stars measured in the field of SL 784.

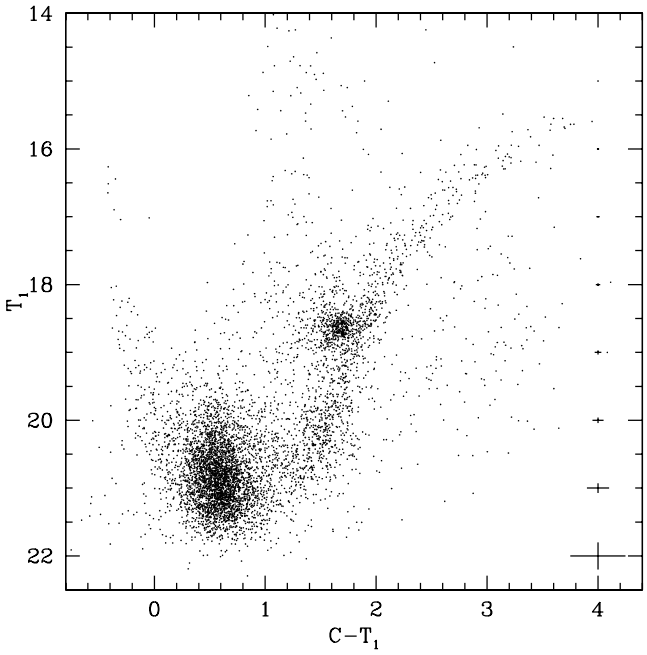

FIG. 3.—$(C - T_1, T_1)$ color-magnitude diagram for all the measured stars in the field of SL 874.

metallicity effects and can even exhibit imperceptible variations for a specific metallicity range within the expected photometric errors. We profited from the available theoretical isochrones computed for the Washington photometric system to estimate cluster ages. Particularly, we used the isochrones calculated by the Padova group (Girardi et al. 2002), including core

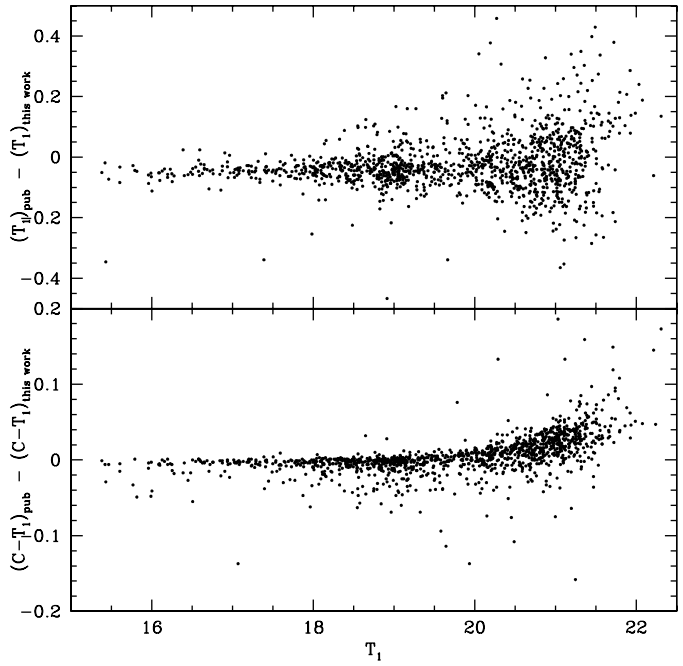

FIG. 2.—Comparison of our photometry with that of Piatti et al. (2007) for L 110 and L 112.

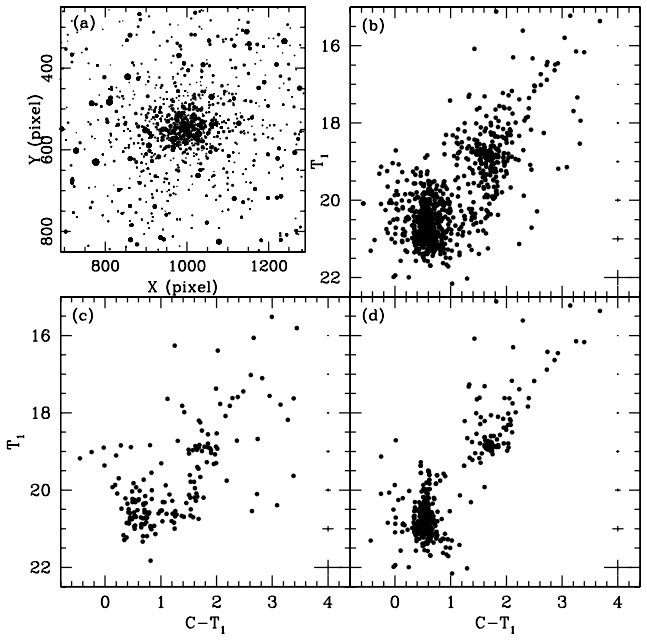

FIG. 4.—(*a*) Schematic finding chart of the stars observed in the cluster field of NGC 2161. North is up and east is to the left. The size of the plotting symbol is proportional to the T_1 brightness of the star. Three extracted CMDs for (*b*) the observed cluster region, (*c*) the equal cluster area surrounding field, and (*d*) the cluster statistically cleaned from field contamination.

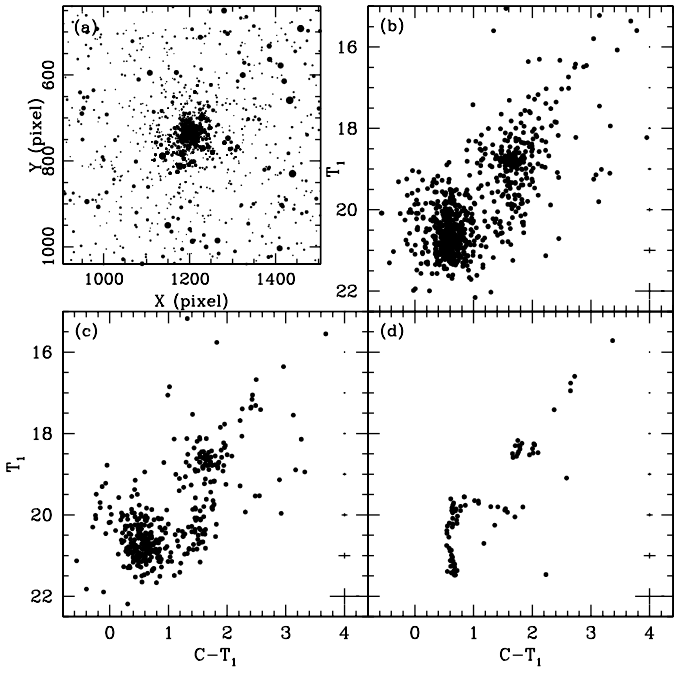

FIG. 5.—(*a*) Schematic finding chart of the stars observed in the cluster field of SL 874. North is up and east is to the left. The size of the plotting symbol is proportional to the T_1 brightness of the star. Three extracted CMDs for (*b*) the observed cluster region, (*c*) the equal cluster area surrounding field, and (*d*) the cluster statistically cleaned from field contamination.

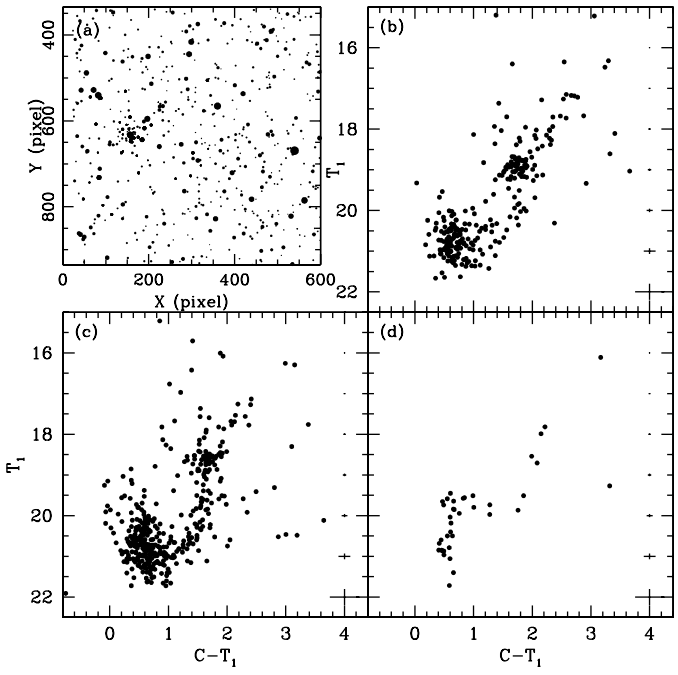

FIG. 6.—(*a*) Schematic finding chart of the stars observed in the cluster field of KMHK 1719. North is up and east is to the left. The size of the plotting symbol is proportional to the T_1 brightness of the star. Three extracted CMDs for (*b*) the observed cluster region, (*c*) the equal cluster area surrounding field, and (*d*) the cluster statistically cleaned from field contamination.

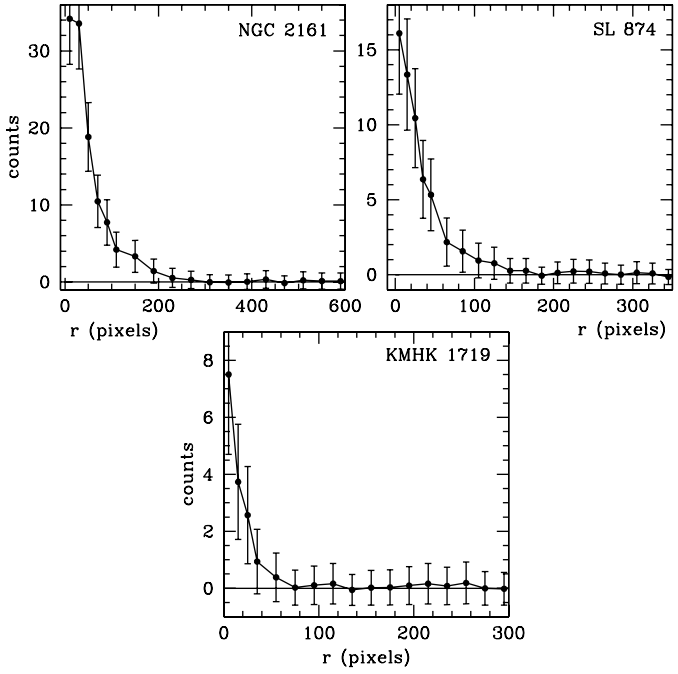

FIG. 7.—Stellar density profiles for the selected clusters, with the Poisson errors included. The horizontal lines correspond to the background levels far from the clusters.

overshooting. These isochrones led to results similar to those that would have been derived if the Geneva group's (Lejeune & Schaerer 2001) had been used. However, the former reach fainter luminosities, thus allowing a better fit to the fainter portions of the MS.

When selecting subsets of isochrones for different Z metallicity values to assess the metallicity effect in the cluster fundamental parameters, we preferred to follow the general rule of starting without assuming any prearranged metallicity. Instead, we adopted chemical compositions of $Z = 0.001$, 0.004, and 0.008 ([Fe/H] $= -1.3$, -0.7, and -0.4, respectively) for the isochrone sets that cover the metallicity range of most of the LMC clusters studied in detail (Piatti et al. 2009). We then selected a set of isochrones, along with the equations $E(C-T_1) = 1.97E(B-V)$ and $M_{T_1} = T_1 + 0.58E(B-V) - (V-M_V)$ (Geisler & Sarajedini 1999), and superimposed them on the cluster CMDs, once they were properly shifted by the corresponding $E(B-V)$ color excesses and by the LMC apparent distance modulus. In the matching procedure, we employed seven different isochrones for each metallicity level, ranging from slightly younger than the derived cluster age to slightly older. Finally, we adopted the cluster age as the one corresponding to the isochrone that best reproduced the cluster main features in the CMD. The presence of RCs and/or RGBs in some cluster CMDs made the fitting procedure easier. We noted, however, that the theoretically computed bluest stage during the He-burning core phase is redder than the observed RC in the CMDs of some clusters, which is a behavior

TABLE 7
CLUSTER SIZES

ID	$r_{\rm FWHM}$ (pixels)	$r_{\rm FWHM}$ (parsecs)	$r_{\rm cls}$ (pixels)	$r_{\rm cls}$ (parsecs)
NGC 2161	50 ± 20	5 ± 2	250 ± 30	24 ± 3
SL 874	30 ± 10	3 ± 1	140 ± 20	14 ± 2
KMHK 1719	20 ± 10	2 ± 1	70 ± 20	7 ± 2

previously detected in other studies of Galactic and Magellanic Cloud clusters (for example, Geisler et al. 2003; Piatti et al. 2004a, 2004b). A similar outcome was found from the fitting of isochrones in the M_V vs $(V-I)_o$ diagram (among others, Piatti et al. 2003b, 2003c). Figure 8 shows the results of the fittings. For each cluster CMD, we plotted the isochrone of the adopted cluster age in solid lines and two additional isochrones bracketing the derived age in dotted lines. The ages of the bracketing isochrones were estimated by taking into account the observed dispersion in the cluster CMDs. We list in Table 8 the ages of the adopted isochrones and the corresponding metallicities for the three studied clusters.

We also derived cluster ages from the δT_1 index, calculated by determining the difference in the T_1 magnitude of the RC and the MS TO in the cluster CMDs. An uncertainty of $<\sigma_{\rm TO}>=0.20$ mag was assigned to the TO T_1 magnitude. In view of the crowded nature of some cluster fields, of the rather sparse RC, and especially of the somewhat subjective nature of this procedure, slightly larger errors may appear. We then derived the cluster ages from the corresponding δT_1 values using equation [4] of Geisler et al. (1997). The resulting values are listed in column (7) of Table 8. As can be seen, they are in good agreement with those derived from the isochrone fittings, which confirms that both methods permit estimating ages in a similar scale. So it was not necessary to apply any zero-point offset. When adding the cluster ages in the results shown in Figure 14 of Mackey & Gilmore (2003), we found that their $r_{\rm FWHM}$ radii fall within the expected range. On the other hand, both methods of estimating cluster ages allowed us to reproduce the cluster age scale of Piatti et al. (2009), which we will adopt in the subsequent analysis on the formation history of the LMC clusters.

We then followed the standard giant branch procedure of adding in the results shown in Figure 4 of Geisler & Sarajedini (1999) the absolute M_{T_1} magnitudes and intrinsic $(C-T_1)_o$ colors for these clusters to roughly derive the cluster metal abundances [Fe/H] by interpolation (Fig. 9). The metallicities herein derived were then corrected for age effects following the prescriptions given in Geisler et al. (2003). Here, we applied a constant correction of $+0.5$ dex. The final age-corrected [Fe/H] values are listed in column (9) of Table 8. We found a good agreement between these values and those corresponding to the isochrones that best resemble the cluster CMDs (column [8] of Table 8). Note that Girardi et al. (2002) models are computed for [Fe/H] $=-1.3$ and -0.7 dex, but not for in-between metallicity values.

5. ANALYSIS AND DISCUSSION

Several observational works have appeared in recent literature that aim at widening the existing knowledge of the line-of-sight depth in the disk and bar region of the LMC (Subramanian & Subramanian 2010), of its galaxy structure (Pejcha & Stanek 2009) and outer limits (Saha et al. 2010), of its hierarchical structure (Bonatto & Bica 2010), of its age-metallicity relation (AMR; Cole et al. 2005), and of its cluster ages (Popescu & Hanson 2010). From a theoretical point of view, Chandar et al. (2010) and de Grijs & Anders (2006) have compared different methods for determining the age distribution of LMC clusters, while Harris & Zaritsky (2009) have reconstructed the SFH of this Galaxy. As far as we know, however, no thorough age distribution study has been recently carried out for the LMC clusters older than 1.0 Gyr. This is the reason why we devote this section to deal with such an issue.

We first searched in the literature for previous LMC cluster age determinations. Next, we added the three clusters studied here to a list of 42 selected LMC clusters older than 1 Gyr that was recently compiled by Piatti et al. (2009, see their Table 9) to produce a cluster list whose ages were determined on as similar of a scale as possible. This age scale is, in turn, that of the present cluster sample. This procedure decreases uncertainties in the fundamental parameter determinations and avoids zero-point offsets between different age scales. Independent age determinations for the total sample of 45 LMC clusters are generally in good agreement. Note that the ages of nine well-known LMC clusters older than 12 Gyr were taken from the literature, rather than derived from Washington photometry. The remaining

TABLE 8
FUNDAMENTAL PARAMETERS OF LMC CLUSTERS

Name	$E(B-V)$ (mag)				Age (Gyr)		[Fe/H]	
(1)	(2)	(3)	(4)	(5)	(6)	(7)	(8)	(9)
	BH	SFD (min)	SFD (max)	Adopted	Isochrone	δT_1	Isochrone	Std GB
NGC 2161	0.12	0.13	0.14	0.13	1.0 ± 0.3	1.2 ± 0.3	−0.7	−0.6 ± 0.2
SL 874	0.09	0.08	0.09	0.09	1.3 ± 0.3	1.6 ± 0.3	−0.7	−0.6 ± 0.2
KMHK 1719	0.09	0.08	0.09	0.09	1.3 ± 0.3	1.5 ± 0.3	−0.7	−0.5 ± 0.2

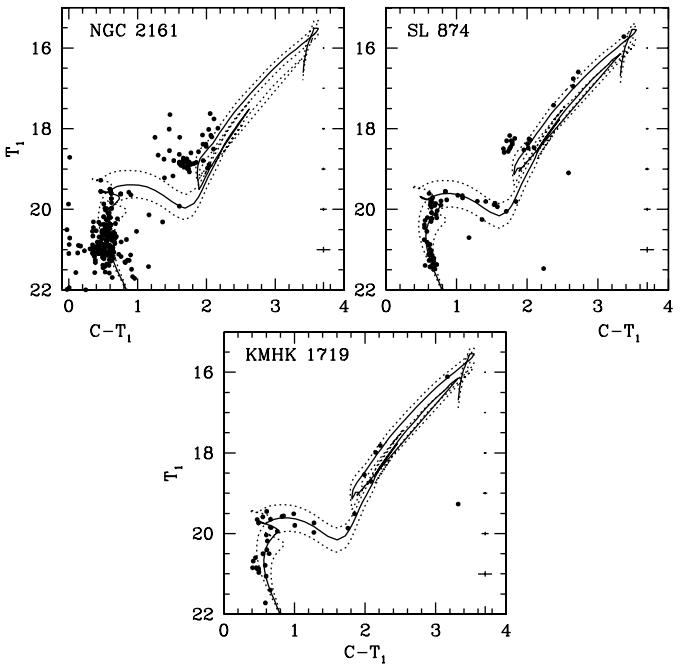

FIG. 8.—Cleaned Washington T_1 vs. $C - T_1$ CMDs for the selected star clusters. Isochrones from Girardi et al. (2002), computed taking into account overshooting are overplotted. The solid and dashed lines correspond to the derived cluster ages and to the ages obtained by taking into account their associated errors (see columns [6] and [8] of Table 8), respectively: $\log(t) = 8.90$, 9.00, and 9.10 and $Z = 0.008$ for NGC 2161 (*upper left*); $\log(t) = 9.00$, 9.10, and 9.20 and $Z = 0.008$ for SL 874 (*upper right*); and $\log(t) = 9.00$, 9.10, and 9.20 and $Z = 0.008$ for KMHK 1719 (*bottom*).

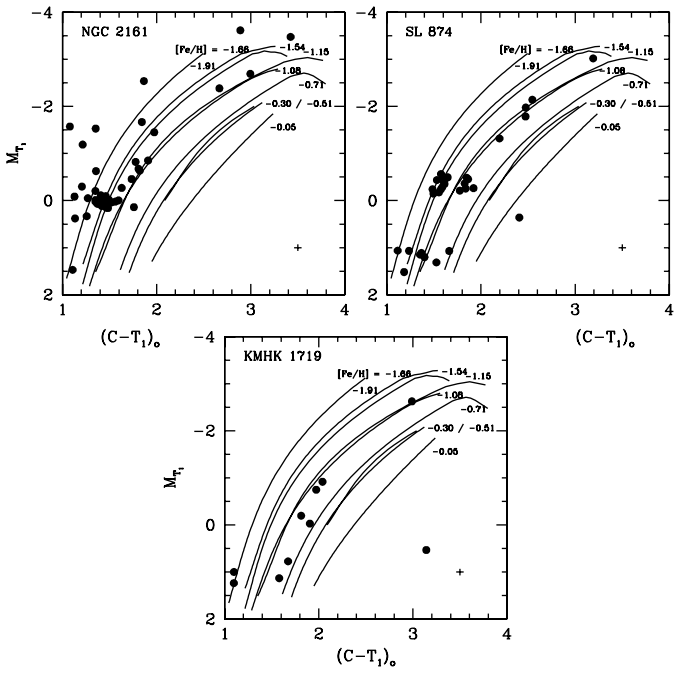

FIG. 9.—Washington M_{T_1} vs. $(C - T_1)_o$ diagram of upper RGB stars in the studied clusters, with standard giant branches from Geisler & Sarajedini (1999) superimposed. Note that an age-dependent correction to the indicated metallicities, as derived in the text, was applied for these clusters.

clusters come from our own studies using the same Washington C and T_1 technique described in this article.

The histogram of the cluster ages is frequently built using a fixed age bin of ~100–500 Myr. This age bin makes it difficult to distinguish any intrinsic fluctuations along the younger cluster range, while the older clusters turn out to be almost subsampled. Piatti (2010) showed that a fixed age-bin size is not appropriate to obtain an intrinsic age distribution, since the result depends on the chosen age interval. A more suitable age interval should be the one whose width is a measure of the cluster age errors in that interval. This would lead to choose very narrow bins for younger clusters and relatively broader age bins for older ones.

With the aim of building an age histogram that tightly reproduces the intrinsic cluster age distribution, we considered the uncertainties in the age estimates to define the age intervals in the whole cluster age range. In this way, we obtained a more appropriate sampling of the clusters per age interval than if we had used a fixed bin size, since we included a number of clusters in each bin whose age errors are close to the size of this bin. In fact, the age errors for young clusters are, in general, a few million years, while those for older clusters are at least a few billion years. Therefore, smaller bins are appropriate for younger clusters, whereas larger bins are suitable for older ones. We then searched the selected cluster age list and found that typical age errors lie in the interval of $0.05 \lesssim \Delta\log(t) \lesssim 0.10$. We built a revised age histogram by setting the bin sizes according to this logarithmic law, which traces the variation in the derived age uncertainties in terms of the cluster ages. We used intervals of $\Delta\log(t) = 0.20$, since if we had used $\Delta\log(t) = 0.10$, we would have obtained a slightly noisier histogram. Thus, the subdivision of the whole age range in age intervals of different sizes can be performed on an observational-based foundation, as they are a measure of the typical cluster age errors for each age range.

In addition to the variation of the age-bin sizes in terms of the estimated age errors, there is another source of uncertainty in the number of clusters per age bin that depends on the age used to define the lower limit of the age histogram. For this reason, we produced four different cluster age histograms with successively starting points at $\log(t) = 8.90$, 8.95, 9.00, and 9.05, respectively. Figure 10 depicts the resulting averaged age histogram with the error bars included. Note that although the four histograms were calculated using bins of $\Delta\log(t) = 0.10$, that of Figure 10 was resampled into 1 Gyr wide bins.

Figure 10 shows that the LMC cluster system seems, at first glance, to have experienced two main formation processes that peaked at $t \sim 2$ and ~13–14 Gyr, respectively, with the former being more prominent and constrained in time. Moreover, tracing the variation of the histogram slope from older to

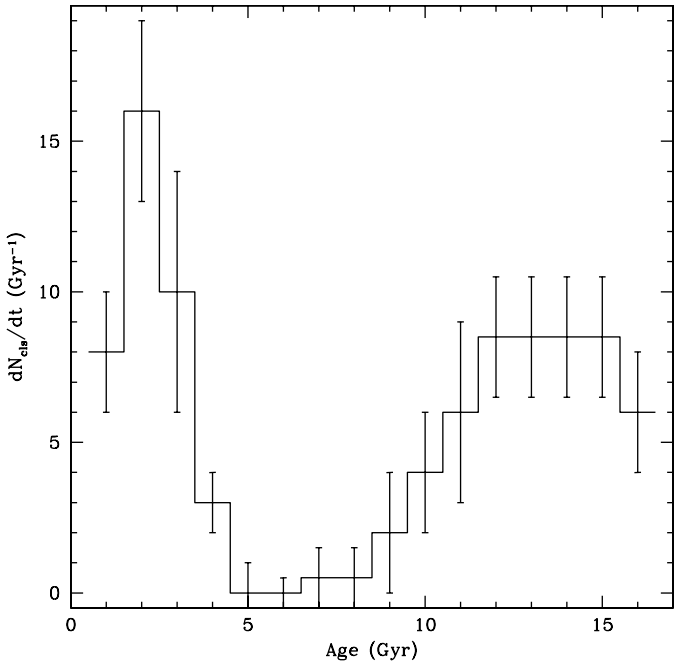

FIG. 10.—The intrinsic age distribution of 45 well-known LMC clusters older than 1 Gyr.

younger ages, we find that after the birth of the LMC cluster system, the galaxy has undergone a decelerating cluster formation period during ∼9 Gyr. Later, at $t \sim 4$ Gyr, the age distribution presents an abrupt change in the slope as a consequence of a sudden appearance of a relative excess of clusters. Such excess could arise from an enhanced cluster formation event triggered by the tidal interaction between both Magellanic Clouds (e.g., Chiosi et al. 2006). On the other hand, although the so-called LMC cluster age gap—precisely the period between the peaks of both formation epochs—is well known to exist, the nuance that the present age histogram brings to light is that it would be more appropriate to refer to it as a decreasing cluster formation rate scenario, rather than as a quiescent period, as it is frequently mentioned in LMC AMR analyses. Indeed, the latter terminology could lead to an idea of inactivity in the LMC, which did not last more than a couple of billion years, if it has ever happened.

Finally, we compared the present cluster age distribution for star clusters older than 1 Gyr with the star formation rates analytically derived by de Grijs & Anders (2006) and Harris & Zaritsky (2009), respectively. The former showed that the cluster formation rate in the LMC has been roughly constant outside the well-known age gap between ∼3 and 13 Gyr, when the cluster formation rate was a factor of ∼5 lower. The least-squares power-law fit for the most likely age ranges where disruption may dominate evolutionary fading derived by them is reproduced at the top panel of Figure 11, wherein we superimposed our Figure 10 properly scaled. As can be seen, the agreement is satisfactory, except as we approach larger ages, where we find

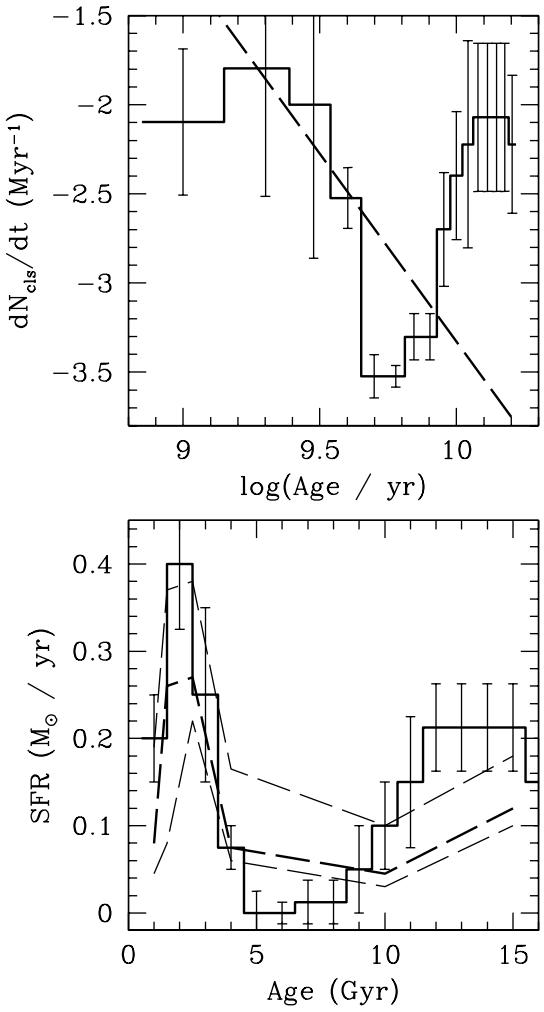

FIG. 11.—Comparison of the derived age distribution for LMC clusters, appropriately scaled, with that by de Grijs & Anders (2006) (*top panel*) and with Fig. 11 by Harris & Zaritsky (2009) (*bottom panel*).

an excess of clusters. This is because de Grijs & Anders (2006) used cluster subsamples. On the other hand, Harris & Zaritsky (2009) presented the first-ever global spatially resolved reconstruction of the SFH of the LMC, based on the application of their StarFISH analysis software to the multiband photometry of 20 million of its stars from the Magellanic Clouds Photometric Survey. The general outlines of their results are consistent with previously published, as well as with the present, results. The bottom panel of our Figure 11 reproduces Harris & Zaritsky's (2009) Figure 11 with our cluster age histogram overplotted, once we converted the total number of clusters formed at each age to stellar masses per year. With dotted lines we represent Harris & Zaritsky's (2009) error bars.

6. SUMMARY AND CONCLUSIONS

In order to complement our Washington photometric studies on intermediate-age and old LMC star clusters, we turned our

attention to the previously unstudied clusters NGC 2161, SL 874, and KMHK 1719. The analysis of the current photometric data leads to the following main conclusions:

1.To disentangle cluster features from those belonging to their surrounding fields, we applied a subtraction procedure to statistically clean the cluster CMDs from field star contamination. The three studied clusters turned out to be relatively small angular-shaped objects.

2.Using the cleaned cluster (T_1, $C - T_1$) diagrams, we estimated ages and metallicities using theoretical isochrones computed for the Washington system. These CMDs are particularly sensitive for metallicity determinations. We also estimated ages from the δT_1 index and metallicities by applying the standard giant branch procedure. The two methods for both age and metallicity determination are in very good agreement with each other. The three clusters are found to be of intermediate-age ($\sim$1 Gyr) and relatively metal-poor ($[\mathrm{Fe/H}] \geq -0.7$ dex).

3.Combining the current results with others available in the literature, we compiled a total sample of 45 well-known LMC clusters older than 1 Gyr. Then, by adopting an age interval varying in terms of age according to a logarithmic law, we built a revised cluster age histogram, which proves to trace the intrinsic cluster age distribution more properly. The revised age distribution can be considered to statistically represent from intermediate-age to old populations.

4.The cluster age distribution of the present study reveals that the LMC cluster system has experienced two main formation episodes that took place $\sim$2 Gyr and $\sim$13–14 Gyr ago. After the birth of the cluster system, the LMC underwent a decelerating cluster formation period that lasted $\sim$9 Gyr. More recently, however, $\sim$4 Gyr ago, an abrupt change in the slope of the cluster age distribution occurred that was probably due to an enhanced cluster formation episode triggered by the tidal interaction between both Magellanic Clouds.

We are gratefully indebted to the Cerro Tololo Inter-American Observatory (CTIO) staff for their hospitality and support during the observing run. This work was partially supported by the Argentinian institutions Consejo Nacional de Investigaciones Científicas y Técnicas, Secretaría de Ciencia y Tecnología de la Universidad Nacional de Córdoba, and Agencia Nacional de Promoción Científica y Tecnológica. This work is based on observations made at CTIO, which is operated by the Association of Universities for Research in Astronomy, Inc., under cooperative agreement with the National Science Foundation. We are very grateful to Peter Stetson for kindly providing the DAOMATCH and DAOMASTER programs.

REFERENCES

Bica, E., Clariá, J. J., Dottori, H., Santos, J. F.C., Jr., & Piatti, A. E. 1996, ApJS, 102, 57
Bica, E., Schmitt, H. R., Dutra, C. M., & Oliveira, H. L. 1999, AJ, 117, 238
Bonatto, C., & Bica, E. 2010, MNRAS, 403, 996
Burstein, D., & Heiles, C. 1982, AJ, 87, 1165 (BH)
Canterna, R. 1976, AJ, 81, 228
Chandar, P., Whitemore, B. C., & Fall, M. 2010, ApJ, 713, 1343
Chiosi, C., Bertelli, G., & Bressan, A. 1988, A&A, 196, 84
Chiosi, E., Vallenari, A., Held, E. V., Rizzi, L., & Moretti, A. 2006, A&A, 452, 179
Cole, A., Tolstoy, E., Gallagher III, J. S., & Smecker-Hane, T. A. 2005, AJ, 129, 1465
de Grijs, R., & Anders, P. 2006, MNRAS, 366, 295
Elson, R. A. W., & Fall, S. M. 1985, ApJ, 299, 211
Elson, R. A. W., Fall, S. M., & Freeman, K. C. 1987, ApJ, 323, 54
Gallart, C. 1998, ApJ, 495, L43
Geisler, D. 1996, AJ, 111, 480
Geisler, D., Bica, E., Dottori, H., Clariá, J. J., Piatti, A. E., & Santos, J. F. C., Jr. 1997, AJ, 114, 1920
Geisler, D., Piatti, A. E., Bica, E., & Clariá, J. J. 2003, MNRAS, 341, 771
Geisler, D., & Sarajedini, A. 1999, AJ, 117, 308
Girardi, L., Bertelli, G., Bressan, A., Chiosi, C., & Groenewegen, M. A. T., et al. 2002, A&A, 391, 195
Harris, J., & Zaritsky, D. 2009, AJ, 138, 1243
Hodge, P. 1988, PASP, 100, 576
Ibata, R. A., Lewis, G. F., & Beaulieu, J.-P. 1998, ApJ, 509, L29
Kontizas, M., Morgan, D. H., Hatzidimitriou, D., & Kontizas, E. 1990, A&AS, 84, 527
Lejeune, T., & Schaerer, D. 2001, A&A, 366, 538
Lauberts, A. 1982, ESO/Uppsala Survey of the ESO (B) Atlas (Garching: ESO)
Lindsay, E. M. 1958, MNRAS, 118, 172
Lyngå, G., & Westerlund, B. 1963, MNRAS, 127, 31
Mackey, A. D., & Gilmore, G. F. 2003, MNRAS, 338, 85
Parisi, M. C., Clariá, J. J., Piatti, A. E., & Geisler, D. 2005, MNRAS, 363, 1247
Pejcha, O., & Stanek, K. Z. 2009, ApJ, 704, 1730
Piatti, A. E. 2010, A&A, 513, L13
Piatti, A. E., Clariá, J. J., & Ahumada, A. V. 2003b, MNRAS, 340, 1249
———. 2003c, MNRAS, 346, 390
———. 2004a, A&A, 418, 979
———. 2004b, A&A, 421, 991
Piatti, A. E., Geisler, D., Bica, E., & Clariá, J. J. 2003a, MNRAS, 343, 851
Piatti, A. E., Geisler, D., Bica, E., Clariá, J. J., Santos, J. F. C., Jr., Sarajedini, A., & Dottori, H. 1999, AJ, 118, 2865
Piatti, A. E., Geisler, D., Sarajedini, A., & Gallart, C. 2009, A&A, 501, 585
Piatti, A. E., Geisler, D., Sarajedini, A., Gallart, C., & Wischnjewsky, M. 2008, MNRAS, 389, 429
Piatti, A. E., Sarajedini, A., Geisler, D., Gallart, D., & Wischnjewsky, M. 2007b, MNRAS, 381, L84
Piatti, A. E., Sarajedini, A., Gallart, C., & Wischnjewsky, M. 2007a, MNRAS, 382, 1203
Popescu, B., & Hanson, M. M. 2010, ApJ, 724, 296

Saha, A., Olszewski, E. W., Brondel, B., Olsen, K., Knezek, P., Harris, J., Smith, Ch., Subramaniam, A., & Claver, J., et al. 2010, AJ, 140, 1719
Schlegel, D. J., Finkbeiner, D. P., & Davis, M. 1998, ApJ, 500, 525 (SFD)
Searle, L., Wilkinson, A., & Bagnuolo, W. 1980, ApJ, 239, 803
Shapley, H., & Lindsay, E. M. 1963, Irish AJ, 6, 74
Stetson, P. B., Davis, L. E., & Crabtree, D. R. 1990, in ASP Conf. Ser. 8, CCDs in Astronomy, (San Francisco: ASP), 289
Subramanian, S., & Subramanian, A. 2009, A&A, 496, 399
———. 2010, A&A, 520, 24
Zaritsky, D., & Lin, D. N. C. 1997, AJ, 114, 2545